Assessing the Provision of Ancillary Services by PV-BES Systems Considering BES Capacity Degradation

Kalliopi D. Pippi, *Graduate Student Member, IEEE,* Georgios C. Kryonidis, *Senior Member, IEEE,* Angelos I. Nousdilis, *Member, IEEE,* and Theofilos A. Papadopoulos, *Senior Member, IEEE*

***Abstract*—The ever-increasing penetration of distributed renewable energy sources, e.g., photovoltaics (PVs), poses new technical challenges, jeopardizing the reliable operation of power systems. For this reason, battery energy storage (BES) are situated alongside PV systems to provide ancillary services (ASs) to system operators. However, BES operation is often limited due to the restricted number of operating cycles. In this paper, a methodology for the assessment of the provision of voltage regulation and power smoothing services by PV-BES systems is presented, taking into account the capacity degradation of BES. The proposed framework involves quasi-static simulations incorporating the operating conditions of the distribution network. A battery aging model is used to estimate the BES capacity loss caused by both the calendar and the cyclic aging mechanisms. The updated BES capacity sets new constraints on its operation and consequently influences the efficiency of the provided ASs. A parametric analysis is conducted to investigate the impact of the most critical parameters on the BES capacity degradation.**

***Index Terms*—Ancillary services, battery energy storage systems, capacity degradation, power smoothing, renewable energy sources, voltage regulation.**

NOMENCLATURE

List of Abbreviations

ASs	Ancillary Services
BES	Battery Energy Storage
BOA	Battery Operating Algorithm
DN	Distribution Network
DoD	Depth of Discharge
DRESs	Distributed Renewable Energy Sources
EoL	End of Life
LV	Low-Voltage
NFECs	Number of Full Equivalent Cycles
POI	Point of Interconnection
PS	Power Smoothing
PVs	Photovoltaics
RRL	Ramp-Rate Limitation
VR	Voltage Regulation

List of Symbols

α_{sei}, β_{sei}	Coefficients of the solid electrolyte interphase BES model
$\Delta\tau$	Time resolution
η_{ch}	Charging efficiency of BES
η_{dch}	Discharging efficiency of BES
$\mathrm{Diff}_{\mathrm{EoL}}$	Difference on the EoL between scenarios
$\overline{SoC}$	Average SoC value
$\overline{T}$	Average battery temperature
$BCAPEX$	BES capital expenditure
$BEMC$	BES equivalent monthly cost
BLV	BES lifetime variation
dr	Monthly discount rate
$E^0_{\max}$	Initial BES capacity
$E^{\mathrm{avail}}_{\mathrm{PS}}$	Available capacity of BES for PS services
$E^{\mathrm{avail}}_{\mathrm{tot}}$	Total available capacity of BES
$E^{\mathrm{cap}}_{\mathrm{PS}}$	Capacity of a BES unit providing PS services
$E^{\mathrm{cap}}_{\mathrm{tot}}$	Nominal capacity of BES
$E^T_{\max}$	Updated available BES capacity at the end of T_{BES}
E_{PS}	Daily profile of the BES energy content for PS
E_{tot}	Overall BES energy content
E_{VR}	Energy of BES for VR provision
E_{bat}	Energy stored in the battery at time instant t
E^{ref}_{bat}	Reference value of energy during PS
f_d	Degradation rate factor of BES
f_{cal}	Calendar degradation factor
f_{cyc}	Cyclic degradation factor
i	Number of charging-discharging cycle
k	Proportional gain
$L^{T_{\mathrm{BES}}}$	Capacity degradation rate over T_{BES}
N	Operating BES cycles within T_{BES}
n	Examined month
P	Output active power of BES for VR
P_{per}	Permissible active power of BES
P_{PS}	Active power of BES for PS at time instant t
P_{VR}	Active power of BES for VR provision at time instant t
$P_{\max}$	Maximum active power of BES
P_{bat}	Charging/discharging power of BES for PS at

The research work was supported by the Hellenic Foundation for Research and Innovation (H.F.R.I.) under the "First Call for H.F.R.I. Research Projects to support Faculty members and Researchers and the procurement of high-cost research equipment grant" (Project Number: HFRI-FM17-229).

K. D. Pippi and T. A. Papadopoulos are with the Power Systems Laboratory, Department of Electrical and Computer Engineering, Democritus University of Thrace, Xanthi 67100, Greece (e-mail: kpippi@ee.duth.gr; thpapad@ee.duth.gr).

G. C. Kryonidis is with the School of Electrical and Computer Engineering, Aristotle University of Thessaloniki, Thessaloniki 54124, Greece (e-mail: kryonidi@ece.auth.gr).

A. I. Nousdilis is with the Department of Electrical and Computer Engineering, University of Western Macedonia, Kozani 50100, Greece (e-mail: a.nousdilis@uowm.gr).

Citation Information: DOI: 10.1109/TIA.2024.3371391

	time instant t
P_{fb}	Feedback power during PS
P_{input}	Power inserted to the RRL control
P_{mpp}	PV output power
P_{sm}	Smoothed PV power
Q	Output reactive power of PV/BES
$Q_{\max}$	Maximum reactive power of PV/BES
RR	Ramp rate of the current time instant t
$RR_{\max}$	Maximum permissible ramp rate
$RR_{\min}$	Minimum permissible ramp rate
$RTVD$	Relative time of violations detection index
S	Rated apparent power of PV/BES
sf	Safety factor
SoC	State-of-Charge
$SoC^{\max}$	Maximum permissible state-of-charge limit
$SoC^{\min}$	Minimum permissible state-of-charge limit
SoC_{bat}^{ref}	Reference SoC level that BES should reach at the end of the PS process
SoC_{init}	Initial SoC value
SoC_{tot}	Daily overall BES SoC profile
SR	Required storage range
t	Examined time instant
T_x^{VV}	Year of the first voltage violation for case x
T_{BES}	Time period of BES aging analysis
T_{LtP}	Elapsed analysis period
$T_{\text{LtP}}^{\max}$	End of the long-term analysis period
T_{qss}	Time period of quasi-static simulations
V	Positive-sequence voltage
$V_{1,\ldots,6}$	Voltage thresholds of the employed droop curves
$V_{\max}$	Maximum permissible voltage limit
$V_{\min}$	Minimum permissible voltage limit

I. Introduction

Currently, the conventional passive distribution networks (DNs) are gradually converted to active systems, due to the advent of distributed renewable energy sources (DRESs), especially photovoltaics (PVs) [1], [2]. This transition from the passive to active operation of DNs contributes to the development of new ancillary services (ASs) that can exploit the functionalities of network assets, e.g., battery energy storage (BES) systems, DRES, etc., to tackle long-term power quality problems related to the steady operation of DNs [3]. Voltage regulation (VR) and active power smoothing (PS) are considered as the most important ASs within the DN premise [4].

Regarding VR, a wide range of VR methods has been proposed in the literature. Most of the works use either the BES active power or the reactive power as the only means for VR. Specifically, in [5] and [6], distributed algorithms are employed to coordinate BES systems in balanced and unbalanced DNs, respectively. Similarly, the use of the reactive power of DRESs and BES systems for VR is assessed in [7] by developing a centralized implementation. An enhanced solution is evaluated in [8], where the well-established $Q(V)$ and $P(V)$ droop-based decentralized control schemes are combined to adjust the active power of BES systems and the reactive power of DRES to control network voltages by prioritizing the use of active against reactive power. However, intense BES utilization for providing ASs has a negative effect on their lifetime expectancy. To reduce BES usage and in turn decelerate BES degradation, recently in [9], a low-complexity, measurement-based VR algorithm is proposed by prioritizing the use of reactive power against the use of the BES active power. An alternative solution involves the use of optimization techniques. Specifically, in [10], [11], the operating setpoints of DRESs and BES systems are optimally determined to control the network voltages using generation and demand forecasts, which, however, may lead to inaccuracies during the real-time operation. To compensate this, an enhanced methodology is proposed [12] where feedback controllers and real-time measurements are used to readjust the operating setpoints. The efficiency of most of the reported VR techniques has been evaluated in [9]. Among the most sophisticated VR methods, the $Q(V) - P(V)$ [8] is the most established also from industrial perspective, as it has been adopted by several manufacturers in commercial converters. However, the effect of the BES operation on the BES aging mechanism has not been extensively investigated in any of the above works. This is taken into account in the optimization-based control schemes of [13], [14], where the BES capacity degradation is indirectly included in the mathematical formulation of the optimization problem by incorporating an equivalent BES aging cost. Nevertheless, the long-term BES capacity degradation has not been examined.

Respectively, various PS techniques have been introduced to mitigate the output power fluctuations caused by the volatile and intermittent operation of DRESs. In [15], a ramp-rate limitation (RRL) method is employed by BES systems, and in [16] a high-pass filter with adjustable cutoff frequency is used to smooth the output power of the DRES and achieve fair SoC sharing among the network BES units. To smooth out solar generated power, a Saviztky-Golay filter is employed in [17], requiring less battery capacity compared to other filtering-based PS methods. The use of several filtering-based algorithms for PS has been evaluated in [18]. However, none of [15] - [18] have taken into account BES capacity degradation. Conversely, a filtering-based PS algorithm combined with a SoC feedback strategy is proposed in [19] with aim to restrict SoC within acceptable limits. In this work the effect of the proposed PS algorithm on the BES lifetime has been also evaluated. In a more detailed analysis, the impact of the most well-established PS methods on the BES system long-term performance has been investigated in [20], [21]. By performing a systematic parametric analysis, it has been shown that the RRL methods outperform the filtering-based techniques in terms of BES sizing, smoothing, and capacity degradation.

The above studies [5]–[21] solely focus on investigating on particular type of AS, while some of them also neglect the BES capacity degradation. The latter is merely done in [22], where the provision of multiple ASs considering BES degradation has been examined, but only from an economic evaluation perspective.

Based on the above discussion, it can be deduced that literature lacks of an assessment framework where the impact of the BES degradation on the long-term performance of the provided ASs can be examined. To fill this gap, this paper investigates the provision of ASs by PV-BES systems within a multi-services perspective. A methodology to evaluate the provision of VR and PS services is proposed. The proposed methodology combines a BES aging analysis methodology with quasi-static simulations to replicate the practical operating conditions of the low-voltage (LV) DN. This is dictated to improve the accuracy of the final evaluation results. The battery degradation model of [23] is adopted to estimate the BES system calendar and cyclic capacity fading, setting in turn technical constraints to BES operation and consequently to the effectiveness of the provided ASs.

A preliminary account of this work has been given in [1]. This paper extends the study of [1] by conducting a systematic parametric analysis to evaluate further the impact of several factors. More explicitly, results are discussed considering different values of BES operating temperature, BES size and simulation time resolution, as well as different BES discharging strategies.

II. Methodology

To evaluate the provision of VR and PS ASs by PV-BES systems to DNs, a quasi-static simulation model is developed. Long-term performance analysis, e.g., 20 years, is conducted on the basis of multiple 24-h time simulations. Special emphasis is given on the modelling endeavor of the BES system by embedding a battery degradation algorithm into the simulation model. Considering the coordination of PS and VR, PS precedes VR in the calculation process. This can be justified by the fact that VR is performed assuming smoothed active power injections by the PV-BES systems. An overview of the proposed methodology is depicted in the flowcharts of Figs. 1 and 2 and in brief involves the following main steps:

- **Step 1**: Import PV, load demand, BES data and DN topology.
- **Step 2**: To alleviate PV output power fluctuations during cloudy days an RRL-based PS algorithm is employed.
- **Step 3**: A day-ahead planning algorithm is applied to estimate the available BES capacity and ensure the effective participation of PV-BES systems in VR actions of the next day.
- **Step 4**: Quasi-static simulations are conducted. To prioritize the provided ASs, a battery operating algorithm (BOA) is deployed. Additionally, the $Q(V) - P(V)$ droop-based algorithm [8], [24] is used to mitigate possible voltage violations.

Steps 1-4 are repeated for a number of days in sequence (See Fig. 2) to create a multi-day simulation pattern of time period T_{qss}.

- **Step 5**: The simulation pattern of T_{qss} is used to evaluate the BES capacity loss [23] (See Fig. 2). The BES aging analysis is conducted regularly with a time period, T_{BES}; T_{BES} can vary from a day to several years depending on the preferred analysis accuracy. The BES capacities are updated and imported in Step 1 to perform the quasi-static simulations required for the next T_{BES}, and the elapsed analysis period (T_{LtP}) is updated accordingly. Note that, if $T_{\text{qss}} < T_{\text{BES}}$, the multi-day pattern is reiterated up to T_{BES}.

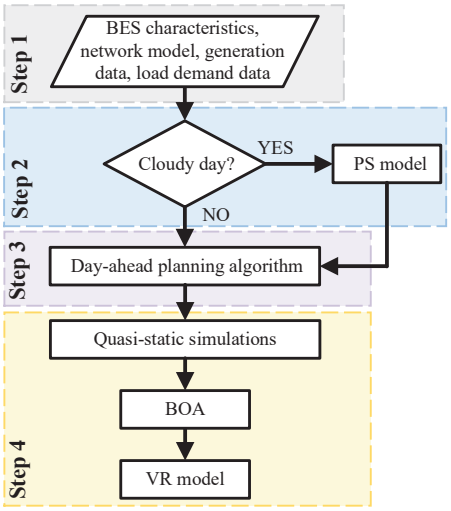

Fig. 1. Flowchart of the proposed methodology (quasi-static simulations).

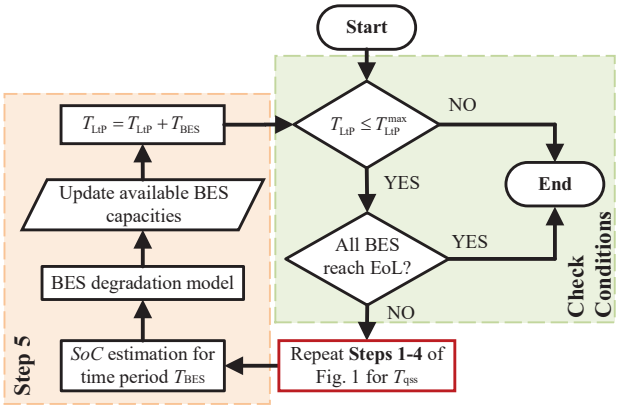

Fig. 2. Flowchart of the proposed methodology (BES aging analysis).

The above procedure is repeated for every T_{BES} till either the end of the long-term analysis period ($T_{\text{LtP}}^{\max}$) is reached or the capacity of all BES units is less than 80 % of their nominal value, indicating their end of life (EoL) [25] (See Fig. 2). In case a BES reaches the EoL earlier than the rest units, it is not considered in the simulation model for the rest of $T_{\text{LtP}}^{\max}$.

A. Power Smoothing Technique

According to the comparative analysis of several PS methods in [20], [21], RRL techniques can assure effective PS, by posing less stress to the battery and in turn prolong its lifetime compared to filtering-based methods. For this reason, in order to smooth out the PV output power fluctuations an enhanced RRL-based method is adopted [15]. The RRL control scheme limits the ramp rate of the PV output power, P_{mpp}^{t}, at each time

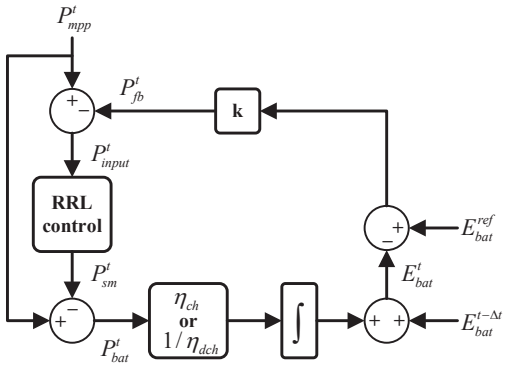

Fig. 3. Enhanced RRL-based PS technique with SoC recovery.

instant, t, to prevent the violation of the maximum, $RR_{\max}$, and minimum, $RR_{\min}$ permissible ramp rates. Assuming that P^t_{input} is the power inserted to the RRL control, the ramp rate of the current time instant, RR^t, is given by (1):

$$RR^t = \frac{P^t_{input} - P^{t-\Delta t}_{sm}}{\Delta t} \tag{1}$$

where $P^{t-\Delta t}_{sm}$ is the smoothed value of the previous time instant. The RRL control calculates the smoothed PV power, P^t_{sm}, that will be injected into the grid as in (2):

$$P^t_{sm} = \begin{cases} P^{t-\Delta t}_{sm} + \Delta t \cdot RR_{\min}, & RR^t \le RR_{\min} \\ P^{t-\Delta t}_{sm} + \Delta t \cdot RR^t, & RR_{\min} < RR^t < RR_{\max} \\ P^{t-\Delta t}_{sm} + \Delta t \cdot RR_{\max}, & RR^t \ge RR_{\max} \end{cases} \tag{2}$$

In this paper, the conventional RRL method is enhanced by introducing a feedback loop [15] to recover the battery SoC towards a pre-specified level, as presented in Fig. 3. This way the BES is always available to smooth out both positive and negative PV output variations. To achieve this, a feedback power, P^t_{fb}, defined in (3), is subtracted from P^t_{mpp} and the resulted power is used as input to the RRL control block.

$$P^t_{fb} = k(E^{ref}_{bat} - E^t_{bat}) \tag{3}$$

Here, k is the proportional gain, E^t_{bat} is the energy stored in the battery at t and E^{ref}_{bat} is a reference value of E^t_{bat} used for SoC recovery, calculated as:

$$E^{ref}_{bat} = \frac{SoC^{ref}_{bat}}{100} E^{\text{cap}}_{\text{PS}} \tag{4}$$

where SoC^{ref}_{bat} stands for the reference SoC level that BES should reach at the end of the PS process and $E^{\text{cap}}_{\text{PS}}$ is the capacity of a BES unit devoted for providing PS services.

The BES charges/discharges accordingly at a rate equal to P^t_{bat} to cover the difference between the actual and the targeted smoothed PV output. The integration of P^t_{bat} considering also the charging or discharging efficiency (η_{ch} or η_{dch}) provides the energy stored to/drained from the battery, that is utilized by the feedback control loop. Finally, based on the estimated E^t_{bat}, the daily profile of the BES energy content (E_{PS}) is acquired.

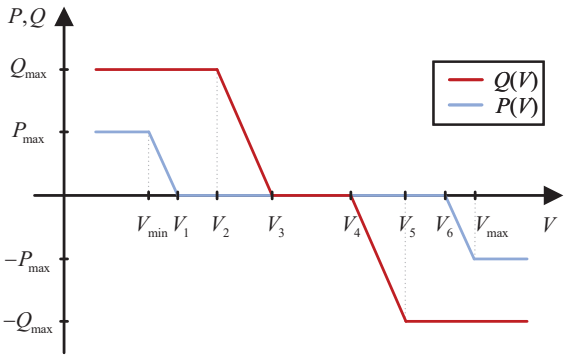

Fig. 4. $Q(V) - P(V)$ droop control curve. A positive P (or Q) value indicates injection to the grid.

B. Voltage Regulation Method

The impact of the provision of VR services on BES capacity degradation is assessed by employing a $Q(V) - P(V)$ droop control scheme in the proposed methodology. The $Q(V) - P(V)$ droop has been considered as one of the most widely-adopted and well-established VR regulation algorithms [8], [24], being also integrated to commercial inverters. In this work, the $Q(V) - P(V)$ control scheme of Fig. 4 is applied to the local controller of the PV-BES systems to regulate the positive-sequence network voltages as imposed by the IEEE 1547 Standard [26]. According to $Q(V) - P(V)$, the output reactive power (Q) of either the PV or the BES and the output active power (P) of the BES are adjusted according to the positive-sequence voltage (V) at the point of interconnection (POI) of each PV-BES system with the grid. Here, V_1, V_2, V_3, V_4, V_5, V_6 denote the voltage thresholds of each droop curve, $V_{\min}$ and $V_{\max}$ stand for the minimum and maximum permissible voltage limits, and $P_{\max}$ and $Q_{\max}$ are the maximum active and reactive power, respectively, that can be used by the BES system and/or the PV. Note that, $P_{\max}$ is determined by the rated power of the BES system, and $Q_{\max}$ is calculated by considering the reactive power capability as follows:

$$Q_{\max} = \sqrt{S^2 - P^2} \tag{5}$$

where S denotes the rated apparent power of either the PV or BES and P is the instant active power of the unit.

Contrary to [8], in the adopted $Q(V) - P(V)$ method priority is given to the use of the reactive power against active power to reduce BES utilization. This is attained by setting narrower voltage thresholds for the activation of the reactive power control ($Q(V)$) compared to the active power control ($P(V)$) as shown in Fig. 4. Regarding [24], the main difference lies on the control of the active power as in [24] PV active power curtailment is applied.

The main triggering signal for the use of the BES system active power in the VR process is the positive-sequence voltage. As no other inputs are used, the method cannot ensure the availability of BESs to provide active power support since their storage capability is limited due to their sizing constraints. To overcome this issue, a day-ahead planning algorithm is adopted aiming to ensure that sufficient amount of energy can

be provided or stored by the BESs during the next day and consequently their effective participation in the VR process. In particular, considering overvoltage mitigation, the proposed algorithm works as follows. Forecasted day-ahead generation and consumption profiles are used in order to perform quasi-static simulations employing the proposed VR method. By the conducted simulations, the required storage range (SR), i.e., the amount of energy that will be stored during the VR process by each BES in the next day, is predicted. To mitigate possible miscalculations caused by the forecast errors a safety factor (sf) is assumed to calculate the final value of SR. Subsequently, a discharging process with constant power is applied to each BES with non-zero SR during no-generation periods to reach the required storing capability. Note that a similar process can be followed for undervoltage mitigation.

C. BES Operating Algorithm

The provision of multiple ASs by the same BES unit necessitates the deployment of BOA to determine the sequence of the provided ASs from the BES.

In this study, the BES unit of Fig. 5 is used. The total available capacity of the BES ($E_{\text{tot}}^{\text{avail}}$) is:

$$E_{\text{tot}}^{\text{avail}} = \frac{SoC_{\max} - SoC_{\min}}{100} E_{\text{tot}}^{\text{cap}} \tag{6}$$

where $E_{\text{tot}}^{\text{cap}}$ is the nominal capacity of the BES unit, $SoC_{\min}$ and $SoC_{\max}$ is the minimum and maximum SoC, respectively. As mentioned above, PS precedes VR in the calculation process. On this basis, $E_{\text{PS}}^{\text{avail}}$, i.e., the available capacity of a BES unit used for PS services, is only a part of the $E_{\text{tot}}^{\text{avail}}$ and coincides with $E_{\text{PS}}^{\text{cap}}$ described in Section II.A. By adopting the PS technique, the daily E_{PS} profile due to PS provision is estimated. From Fig. 5, it is shown that at the end of the PS process, E_{PS} is equal to E_{bat}^{ref}, i.e., the energy value calculated according to (4). Since PS is achieved, the employed VR method is activated. For each time-instant t, the active power for VR provision (P_{VR}^{t}) should satisfy the condition of (7), to assure that the operating characteristics of BES are not violated.

$$P_{\text{VR}}^{t} \leq P_{\text{per}} - P_{\text{PS}}^{t} \tag{7}$$

Here, P_{PS}^{t} is the BES active power utilized for PS and P_{per} is the permissible active power of the BES unit. As both P_{VR} and P_{PS} daily profiles are estimated, the overall BES energy content (E_{tot}) is:

$$E_{\text{tot}} = E_{\text{VR}} + E_{\text{PS}} \tag{8}$$

where E_{VR} is the BES energy used for VR provision.

Finally, the daily overall BES SoC profile (SoC_{tot}) is calculated as $SoC_{\text{tot}} = 100 \cdot E_{\text{tot}} / E_{\text{tot}}^{\text{cap}}$ and SoC_{tot} is used to estimate the BES aging utilizing the BES capacity degradation mechanism described in the following section.

D. BES Degradation Model

The algorithm for the evaluation of the battery degradation within time period T_{BES} is illustrated in Fig. 6. The aging model of [23] for lithium-ion batteries is adopted to assess

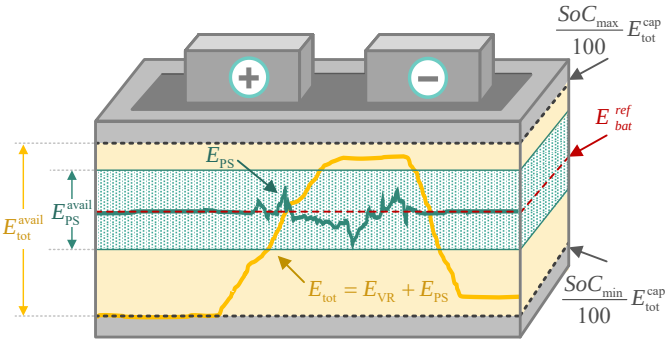

Fig. 5. BES operation diagram.

the capacity loss, considering both the calendar and the cyclic aging process of the battery cells. The calendar aging mechanism over period T_{BES} is modeled by the calendar degradation factor, f_{cal}, and is a function of the average SoC ($\overline{SoC}$) and the average battery temperature ($\overline{T}$) over T_{BES}. The cyclic degradation over the i-th charging-discharging cycle, f_{cyc}^{i}, depends on the depth of discharge (DoD), the $\overline{SoC}$, and the $\overline{T}$ of the cycle. The cyclic aging within T_{BES} is calculated as the sum of the capacity degradation caused by all cycles within T_{BES}. The DoD, the $\overline{SoC}$, the $\overline{T}$ of each cycle and the total number of irregular cycles are determined from SoC timeseries by using the rainflow algorithm [27]. Finally, the capacity degradation rate over T_{BES}, $L^{T_{\text{BES}}}$, is obtained by (9):

$$L^{T_{\text{BES}}} = 1 - \alpha_{sei} e^{-\beta_{sei} f_d} - (1 - \alpha_{sei}) e^{-f_d}. \tag{9}$$

where α_{sei} and β_{sei} are parameters determined by experimental data and f_d is the overall degradation factor, calculated according to (10), for all cycles N within T_{BES}.

$$f_d = f_{cal} + \sum_{i}^{N} f_{cyc}^{i} \tag{10}$$

The analysis of the capacity fading is conducted at the end of each time period T_{BES} and the updated available capacity ($E_{\max}^{T}$) is derived by:

$$E_{\max}^{T_{\text{BES}}} = (1 - L^{T_{\text{BES}}}) E_{\max}^{0} \tag{11}$$

where $E_{\max}^{0}$ is the initial BES capacity.

III. System Under Study

To evaluate the performance of the PS-VR methodology, simulations are conducted using the IEEE European LV test feeder [28]. The original test feeder is modified by adding 32 PV-BES systems; the single-line diagram of the network is depicted in Fig. 7. Two groups of PV-BES systems have been considered, namely, BT1, where PV-BES units are exclusively used for PS and BT2, where PV-BES provide both PS and VR AS. The connection node and the capacity of PVs and BES are summarized in Tables I and II, respectively. Regarding the PV-BES operating characteristics, the nominal power factor of PVs and BESs is considered equal to 0.85, $SoC_{\min}$ and

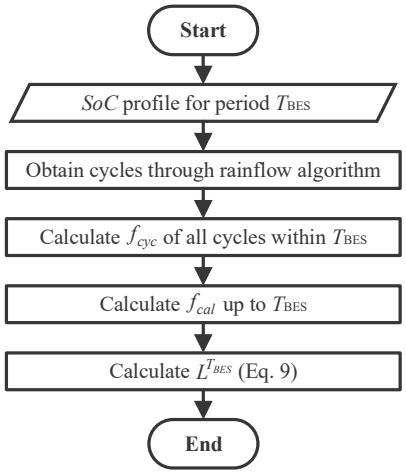

Fig. 6. Algorithm for the analysis of BES capacity degradation.

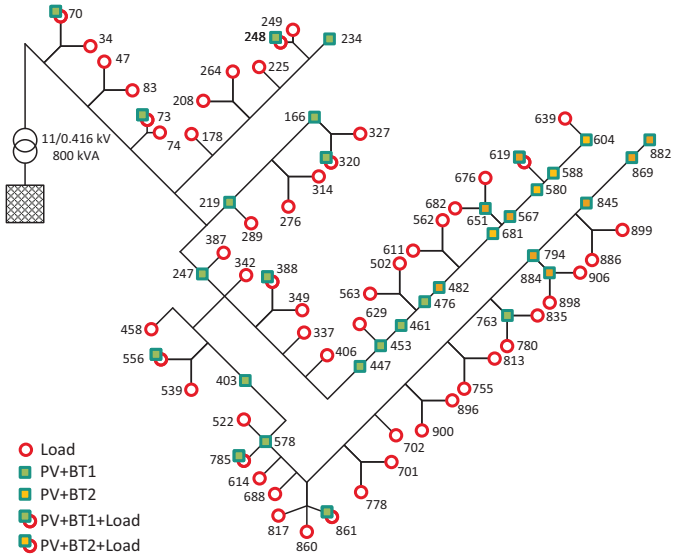

Fig. 7. Single-line diagram of the modified IEEE LV test feeder.

$SoC_{\max}$ of the BESs are 10 % and 90 %, respectively; the charging/discharging efficiency is 0.95.

Moreover, the long-term impact of the ASs on the BES capacity degradation is investigated for $T_{\text{LtP}}^{\max} = 20$ years by adopting the framework described in Section II. In particular, quasi-static simulations are performed in OpenDSS [29] on the basis of multiple 24-h time simulations (Fig. 1). The BES capacity degradation is evaluated considering $T_{\text{BES}} = 1$ year (Fig. 2). A six-day simulation pattern ($T_{\text{qss}} = 6$ days) is reiterated up to 365 days for every year T_{LtP} of the analysis: 24-h sunny and cloudy PV generation profiles with 1-min resolution are used ($\Delta\tau = 1$ min). During a sunny day, the units of BT2 are employed to tackle voltage violations, and the units of BT1 remain idle. On the other hand, on a cloudy day, BT1 units are used for PS and BT2 units provide both PS and VR services. The annual cloudy to sunny days ratio is considered 33.3 %, i.e., two cloudy days within the six-day simulation pattern. In the conducted analysis, 55 load and 2 generation profiles are used from [28] and [20], respectively.

Considering the day-ahead planning algorithm, $sf = 20$ %

TABLE I
PVs Installed Capacity

Node	kWp
70, 166, 234, 247, 248, 388, 403, 447, 453, 482, 556, 567, 580, 588, 619, 651, 763, 785, 845, 861, 869, 884	7.5
73, 219, 320, 461, 476, 578, 604, 681, 794, 882	15

TABLE II
BESs Installed Capacity

BT1		
Node	**kWh**	**kW**
73, 219, 320, 461, 476, 578	3	4.5
70, 247, 166, 234, 248, 388, 403, 447, 453, 556, 785, 763, 861	1.5	2.25

BT2					
Node	**kWh**	**kW**	**Node**	**kWh**	**kW**
482, 681, 845	10	5	882	25	12.5
567, 580, 588	22.5	7.5	604	45	15
619, 651	30	7.5	794	5	5
869	15	7.5	884	5	2.5

and the available load demand profiles are randomly assigned at network load nodes to emulate the stochastic behaviour of LV consumers. The peak load demand of each node is maintained equal to the original one [28]. Regarding generation profiles, a uniform noise within the range of ± 5 % is added to the actual adopted profiles. The capacity degradation of each BES for T_{BES} is determined considering an indicative $\overline{T}$ value equal to 20 °C. Regarding the properties of the examined PS and VR control strategies, it is assumed that the preferred SoC value at the end of the PS method is $SoC_{bat}^{ref} = 50$ %, $k = 2$, $RR_{min} = -1.5$ W/s, $RR_{max} = 1.5$ W/s, $V_{\min}$ and $V_{\max}$ are 0.9 pu and 1.1 pu, respectively, and $V_1 = V_2 = 0.91$ pu, $V_3 = 0.92$ pu, $V_4 = 1.08$ pu, $V_5 = V_6 = 1.09$ pu. Note that the parameters described in this Section pertain to the baseline scenario.

IV. Results and Discussion

In this section, the long-term impact of the BES capacity degradation to the provided ASs is discussed via quasi-static simulations. A parametric analysis is conducted to evaluate the effect of the $\overline{T}$, the SoC_{bat}^{ref}, the discharging strategy, the BES sizing characteristic and the time resolution of the analysis on the BES aging mechanism and consequently on the provided ASs.

A. Long-term Assessment

By using the baseline simulation parameters, the long-term performance of the provided PS and VR services is assessed. Initially, the daily SoC profiles for the BT1 unit situated at node 73 (BT1-73) during a cloudy day of the 1st and the 12th year of the analysis are presented in Fig. 8a. It can be observed that the initial SoC (SoC_{init}) of both curves is 50 %. During the day, BT1-73 provides PS services and the SoC varies from 30 % to 60 %. Due to the SoC recovery signal, the SoC value at the end of the PS method, i.e., SoC_{bat}^{ref}, is equal to SoC_{init} and the $\overline{SoC}$ value is 50 %. The impact of BT1-73 operation

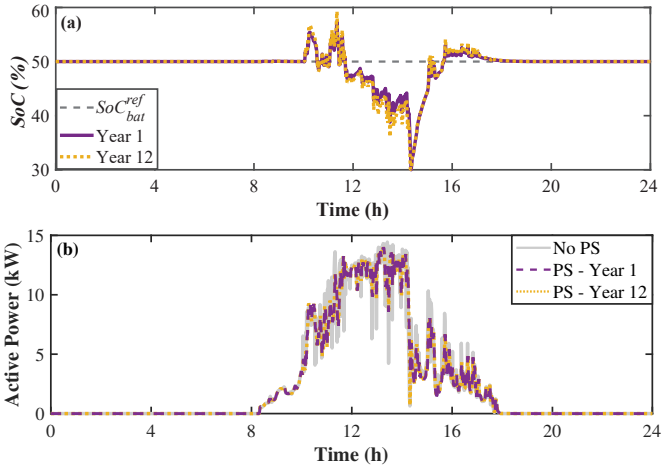

Fig. 8. (a) Daily SoC profile of BT1-73, and (b) daily PV output power profile during a cloudy day.

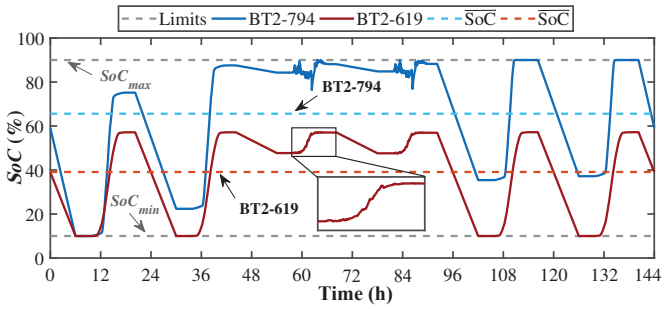

Fig. 9. Six-day SoC profile of indicative BT2 units.

on the PV smoothed output power is depicted in Fig. 8b. It can be generally seen that similar PS is achieved for the 1st and the 12th year, since the two smoothed profiles almost overlap. The small differences between the corresponding curves in Figs. 8a and 8b are because of the battery degradation through the years. Similar remarks are also derived for the rest BT1 units.

In Fig. 9, the SoC profiles of two indicative BT2 units are plotted for a six-day period of the 1st year. In particular, the SoC fluctuations observed in Fig. 9 during 56-66 h and 80-90 h are due to the provision of PS services during a cloudy day. The BES system of node 619 (BT2-619) presents a smoother SoC profile than the BT2 situated at node 794 (BT2-794). This is attributed to the fact that less active power is required by BT2-619 for PS compared to that for VR as this node is one of the most sensitive network nodes in terms of voltage variations. It can be also realized that the SoC profile is influenced by the forecasting load demand and generation error of the day-ahead planning algorithm used for the discharging process. More explicitly, as the load demand and generation forecasts for node 619 are on the safe side, BT2-619 sufficiently discharges and can absorb the required energy for the next day VR process. This entails a $\overline{SoC} = 39.12$ % over the six-day analysis period and consequently on annual basis. However, this is not the case for BT2-794. The inaccurate prediction of the load demand and generation, results into an increased SoC, e.g., after 36 h,

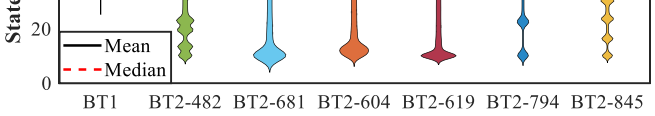

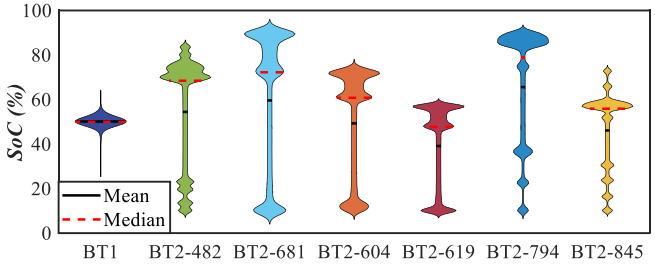

Fig. 10. SoC of indicative BES units.

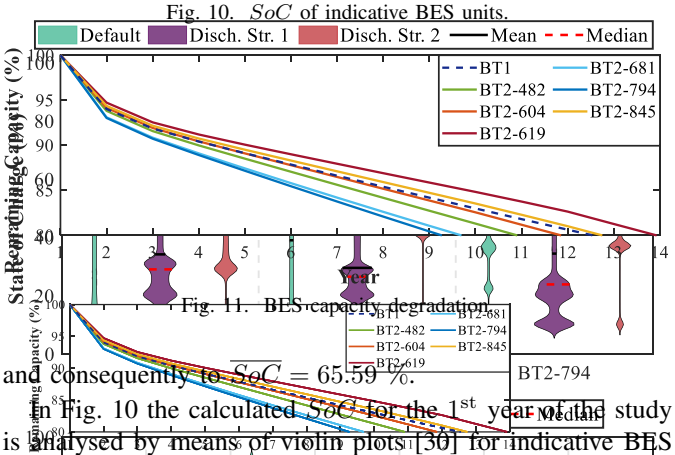

Fig. 11. BES capacity degradation.

and consequently to $\overline{SoC} = 65.59$ %.

In Fig. 10 the calculated SoC for the 1st year of the study is analysed by means of violin plots [30] for indicative BES units; similar results are also derived for the rest years of the analysis. In these plots, the mean and the median SoC are also depicted. It can be seen, that the majority of the plots do not follow a normal distribution with the exception of the BT1 violin plot. In particular, BT2 SoC distributions do not follow a similar pattern as BT2 units operation is significantly influenced by the voltage sensitivity of the POL node. BT2 results also indicate that their $\overline{SoC}$ significantly differs and this is because it strongly depends on the BES size of each unit. The smaller the BES size is, the wider the SoC operating range and the higher the $\overline{SoC}$. This is also substantiated by comparing the corresponding curves of BT2-794 and BT2-619 in Figs. 9 and 10. Finally, from Figs. 8a, 9 and 10, it can be deduced that BT1 units present lower SoC variations than BT2. This is owed to the distinct decreased amounts of storage capacity required for PS compared to VR.

In Fig. 11, the capacity degradation of indicative BT1 and BT2 BESs is analysed. With respect to the results of Figs. 9 and 10, it can be inferred that higher $\overline{SoC}$ operating values and wider SoC operating range lead to accelerated BES aging. Specifically, BT2-794 reaches its EoL at the 9th year, while for BT2-619 a longer lifetime is calculated (up to 14 years), due to the lower $\overline{SoC}$. As BT2-794 and BT2-619 present the highest and the lowest $\overline{SoC}$ of all BES units, i.e., 65.59 % and 39.12 %, respectively, it can be deduced that the available capacity of all BES units is reduced by 20 % after 9-14 years. It is worth noting that the BT2-619 curve presents a slope change after the 12th year. In fact, the BES capacity reduces with a rate of 1.09 % per year up to the 12th year. After this year, most BT2 units have already reached their EoL (11 out of 13), and this entails a need for increased support for VR by BT2-619 and consequently a higher degradation rate, i.e., 1.37 % per year. By comparing the degradation rate of

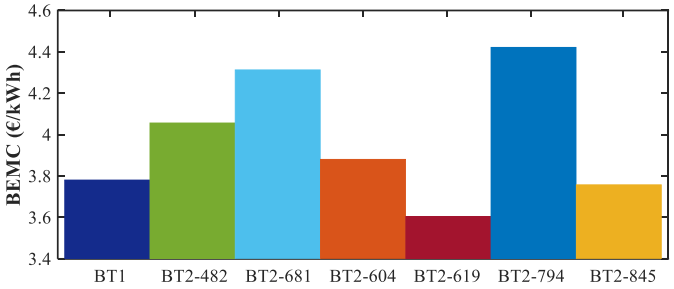

Fig. 12. $BEMC$ for indicative BES units.

BT1 and BT2 units, it can be seen that the provision of both PS and VR services does not explicitly result into decreased BES lifetime expectancy, e.g., BT2-619, BT2-845, compared to BT1 units.

Further, the provision of ASs by BES units is also evaluated in monetary terms. Specifically, by solving (12), the BES equivalent monthly cost ($BEMC$) is calculated for each BES unit [31]. This is the cost of owning and operating a BES unit for each month n and is used as a common basis for comparison to evaluate the cost-effectiveness of BES units with unequal lifespans.

$$BCAPEX = \sum_{n=1}^{\text{EoL}} \frac{BEMC}{(1+dr)^n} \tag{12}$$

Here, $BCAPEX$ is the BES capital expenditure taken equal to 310 €/kWh, assuming a value-added tax of 24 % [32]; dr stands for the monthly discount rate and is set equal to 0.908% corresponding to an effective annual discount rate of 6%. In Fig. 12, the estimated $BEMC$ is illustrated by means of bargraphs for indicative BES units. Considering the BES capacity degradation results of Fig. 11, it can be realized that $BEMC$ is indirectly related with the estimated BES lifetime. More particularly, BES units presenting decelerated BES aging, e.g., BT2-619, show a lower $BEMC$ to those reaching their EoL earlier, e.g., BT2-794 (for BT2-619 and BT2-794 $BEMC$ is 3.61€/kWh and 4.42€/kWh, respectively).

Finally, in Figs. 13a and 13b, the daily profiles of the positive-sequence voltage at node 619 for different years are plotted for sunny and cloudy days, respectively. Differences in the voltage profiles of Fig. 13a during 20:25 h - 07:00 h, are due to the discharging process of BT2. In general, overvoltages are effectively mitigated during the 1^{st} year. Nevertheless, voltage violations are observed at the 12^{th} and 13^{th} year. This is attributed to the fact that most BT2 storage units (11 out of 13) have reached their EoL. Comparing a sunny to a cloudy day, it can be seen that overvoltages are more likely to be tackled in the latter case. Finally, the weakness of BT1 and BT2 to provide PS services during a cloudy day of the 13^{th} year is reflected to the corresponding voltage profiles characterized by intense fluctuations.

B. Effect of Operating Temperature

A parameter of utmost importance that influences the BES degradation mechanism is $\overline{T}$. To elucidate this, additional

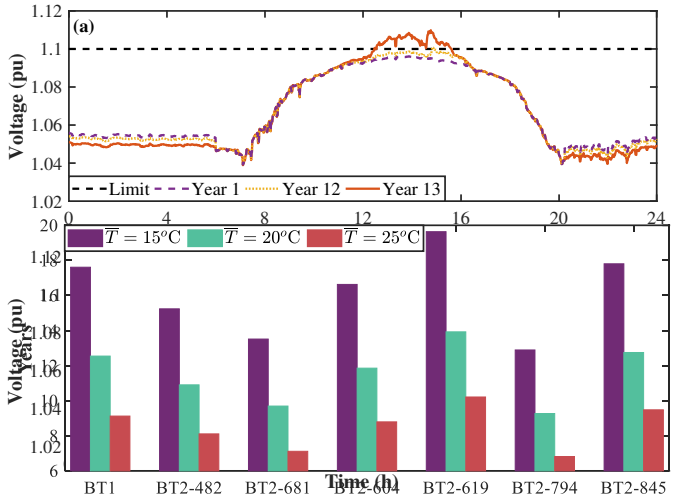

Fig. 13. Voltage profile of node 619 during (a) a sunny and (b) a cloudy day.

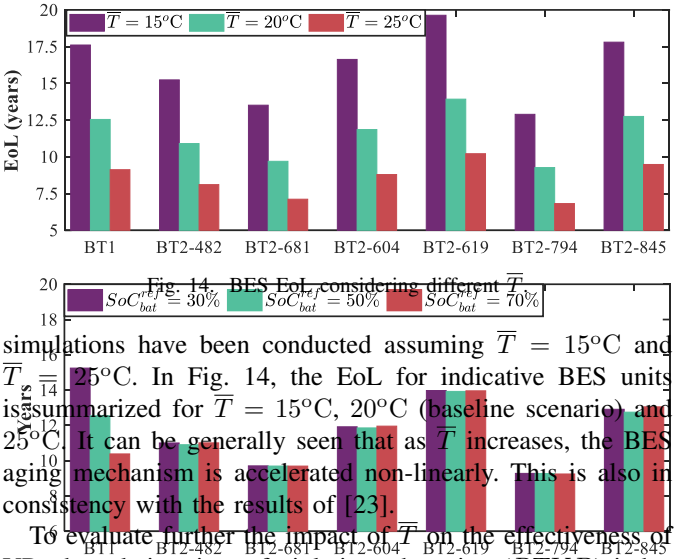

Fig. 14. BES EoL considering different $\overline{T}$.

simulations have been conducted assuming $\overline{T}$ = 15°C and $\overline{T}$ = 25°C. In Fig. 14, the EoL for indicative BES units is summarized for $\overline{T}$ = 15°C, 20°C (baseline scenario) and 25°C. It can be generally seen that as $\overline{T}$ increases, the BES aging mechanism is accelerated non-linearly. This is also in consistency with the results of [23].

To evaluate further the impact of $\overline{T}$ on the effectiveness of VR, the relative time of violations detection ($RTVD$) index defined in (13) is introduced. In essence, $RTVD$ compares the year (T_x^{VV}) when the first voltage violation in the grid occurs with respect to the baseline scenario ($T_{\text{baseline}}^{\text{VV}}$).

$$RTVD(\%) = \frac{T_x^{\text{VV}} - T_{\text{baseline}}^{\text{VV}}}{T_{\text{baseline}}^{\text{VV}}} 100\ \% \tag{13}$$

Here, T_x^{VV} includes cases $\overline{T}$ = 15° C and $\overline{T}$ = 25° C.

The extended BES lifetime for $\overline{T}$ = 15° C results into $RTVD$ = 41.66 % > 0, indicating that voltage violations are observed at a later year compared to $\overline{T}$ = 20° C and consequently enhanced grid performance. For $\overline{T}$ = 25° C, violation events are detected earlier than the 12^{th} year of $\overline{T}$ = 20° C ($RTVD = -25$ %) as less BT2 units are available to provide VR services due to the accelerated BES aging.

C. Effect of SoC Recovery Mechanism

The effect of SoC_{bat}^{ref} on BES aging and grid performance is investigated considering also the 30 % and 70 % cases.

In Fig. 15, violin plots are used to analyze the distribution of the resulting SoC for three indicative BES units. The corresponding EoL is depicted in Fig. 16. It can be seen

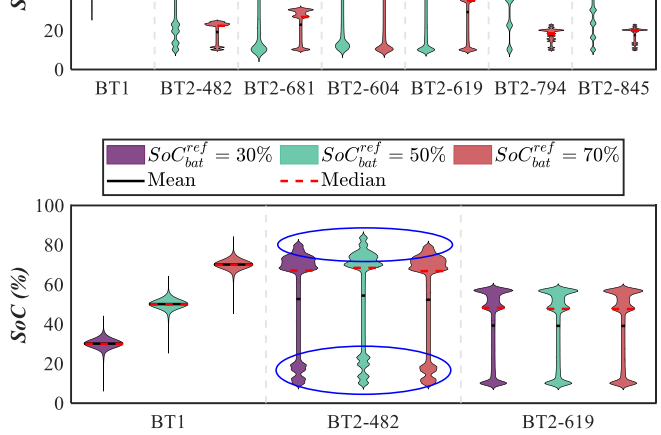

Fig. 15. SoC of indicative BES units for different SoC_{bat}^{ref}.

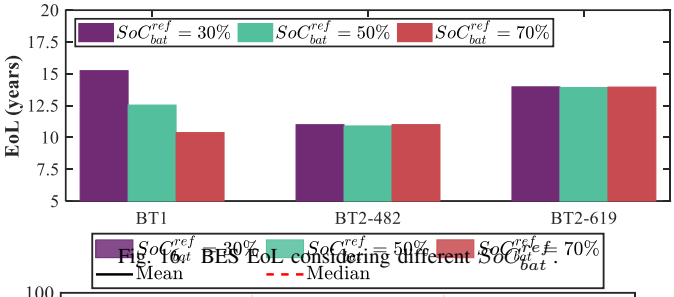

Fig. 16. BES EoL considering different SoC_{bat}^{ref}.

that the influence of the SoC_{bat}^{ref} on the SoC distribution, and consequently on BES lifetime, of BT1 units is more marked than of BT2 units. This is attributed to the fact that the SoC recovery mechanism is only applied to E_{PS} which, contrary to BT1 units, where $E_{\mathrm{tot}} = E_{\mathrm{PS}}$, covers a small part of the overall BES energy content (E_{tot}) in BT2 units (see Sections II.A and II.C). This is also substantiated by $RTVD$ calculations where $RTVD = 0\%$ for both $SoC_{bat}^{ref} = 30\%$ and 70 % cases implying that SoC_{bat}^{ref} has a trivial impact on the grid performance in terms of voltage violations. On the contrary, as SoC_{bat}^{ref} increases, BT1 units operate at higher SoC range (Fig. 15) and this entails decreased BES lifetime (Fig. 16).

It should be also indicated that the small differences in the SoC distribution of BT2-482 marked within blue circles in Fig. 15 are due to the forecast errors of the day-ahead planning algorithm, that result in different discharging BES profiles and in turn to different SoC values. This is also reflected in the corresponding aging results in Fig. 16, where small differences in BT2-482 lifetime are observed.

D. Effect of Discharging Strategy

To assess the impact of the adopted discharging strategy (DS) on the BES lifetime, apart from the baseline discharging strategy (DS1), two additional planning algorithms are considered for BT2 units, namely DS2 and DS3. Scope of DS2 is to achieve lower SoC values compared to DS1, by fully discharging the BT2 units up to $SoC_{\min}$ at the end of each day. Note that in case of a cloudy day, BT2 units are discharged up to 20 % to ensure BES availability for PS provision. DS3 follows a similar rationale to DS1 focusing also on decreasing BT2 utilization. This is attained by activating the discharging process only if the available BES capacity is not adequate to cover the VR needs of the next day.

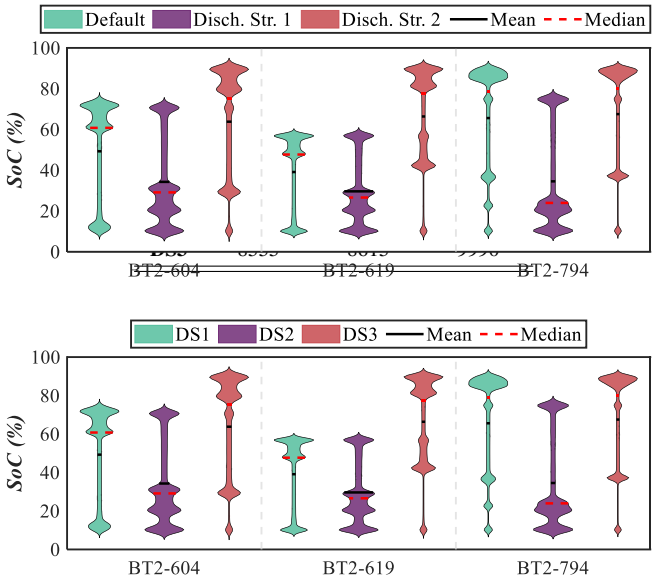

Fig. 17. SoC of indicative BES units for different discharge strategies.

Assuming three indicative BT2 units, the number of full equivalent cycles (NFECs) of the 1st year as calculated by the rainflow algorithm of [27] and the corresponding violin plots of the operating SoC are presented in Table III and Fig. 17, respectively. Furthermore, Fig. 18 presents the difference on the EoL ($\mathrm{Diff}_{\mathrm{EoL}}$) between the examined discharging strategies (DS2 or DS3) and the baseline scenario (DS1), calculated by:

$$\mathrm{Diff}_{\mathrm{EoL}} = \mathrm{EoL}_{SoC_{bat}^{ref}=x\%}^{\mathrm{DS2\ or\ DS3}} - \mathrm{EoL}_{SoC_{bat}^{ref}=x\%}^{\mathrm{DS1}} \quad (14)$$

According to Table III, it can be observed that the adopted discharging strategy has a negligible impact on the NFECs ranging from 0 % to 1.4 % with respect to DS1. On the contrary, the operating SoC is significantly influenced by the discharging mechanism, and this is also reflected on the BES lifetime as shown in Figs. 17 and 18, respectively. Specifically, BES aging is accelerated in case of DS3 ($\mathrm{Diff}_{\mathrm{EoL}} < 0$), as it leads to a wider operating range with increased SoC values compared to DS1. Moreover, DS2 outperforms DS1 and DS3 in terms of both BES lifetime expectancy ($\mathrm{Diff}_{\mathrm{EoL}} > 0$) and grid performance ($RTVD = 16.66$ %), as it forces BT2 units to operate with decreased SoC values. Based on the above, it can be inferred that contrary to NFECs, the operating SoC can be used as a reliable index to assess the impact of the discharging mechanism on the BES lifetime.

E. Effect of BES Sizing

The influence of BES sizing on the BES aging mechanism is also assessed by increasing the installed BES capacity of the baseline scenario and setting it equal to 45 kWh for all BES units. Note that, some BES units present the same BES capacity in the two cases.

The operating SoC and the BES lifetime variation (BLV) of seven indicative BES units are depicted in Figs. 19 and 20, respectively. BLV is defined as the percentage variation

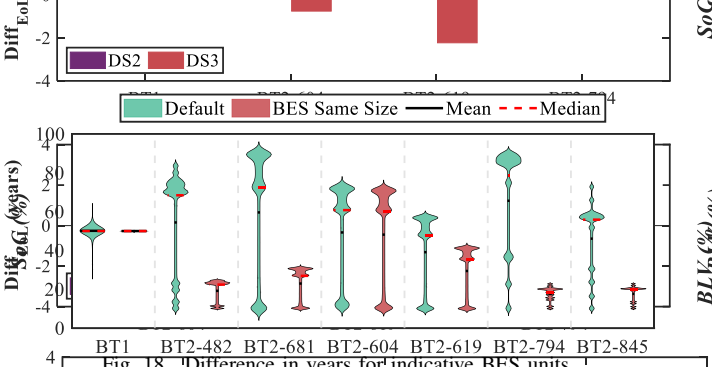

Fig. 18. Difference in years for indicative BES units.

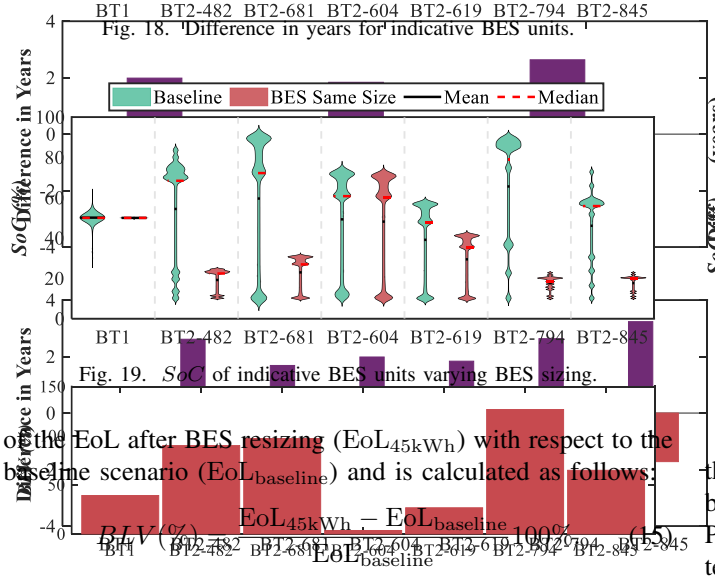

Fig. 19. SoC of indicative BES units varying BES sizing.

of the EoL after BES resizing ($\mathrm{EoL}_{45\mathrm{kWh}}$) with respect to the baseline scenario ($\mathrm{EoL}_{\mathrm{baseline}}$) and is calculated as follows:

$$BLV\,(\%) = \frac{\mathrm{EoL}_{45\mathrm{kWh}} - \mathrm{EoL}_{\mathrm{baseline}}}{\mathrm{EoL}_{\mathrm{baseline}}} 100\% \quad (15)$$

In case of equal BES sizing, the SoC profile of BT1 units is squeezed around 50 % as shown in Fig. 19. This is attributed to the fact that E_{PS} remains constant as the installed BES capacity is increased with respect to the baseline scenario. Additionally, as the capacity of BT2 units is increased to 45 kWh, the operating SoC range is reduced which in turn extends the BES lifetime reaching BLV values up to 125% (see Fig. 20). Note that the operating SoC range and lifetime of BT2-604 remain almost unaffected since the installed capacity is equal to 45 kWh for both examined scenarios. Moreover, the deceleration of BES aging extends the provision of VR and PS services to a longer time period, e.g. $RTVD = 50$ %, compared to the baseline scenario, improving the overall network performance. This is an important outcome that must be considered by the distribution system operator during the planning stage where a trade-off must be found between cost that is mainly driven by the BES sizing and network performance that is affected by the BES lifetime.

F. Effect of Time Resolution

To evaluate the effect of time resolution ($\Delta\tau$) on the performed calculations, additional simulations are conducted by assuming $\Delta\tau = 10$ min. Note that in the baseline scenario $\Delta\tau = 1$ min. The $\mathrm{Diff}_{\mathrm{EoL}}$ for the examined scenarios is depicted in Fig. 21 for seven indicative BES units. It can be seen that increased $\Delta\tau$ overestimates the BES lifetime compared to the baseline scenario. Nevertheless, this is a spurious observation which is attributed to the fact that as $\Delta\tau$ increases, valuable information regarding network behavior and BES operation is lost and is not considered in the BES aging mechanism, which in turn overestimates BES EoL.

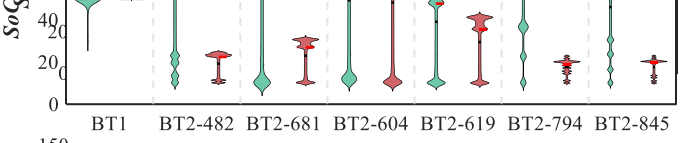

Fig. 20. BLV for indicative BES units.

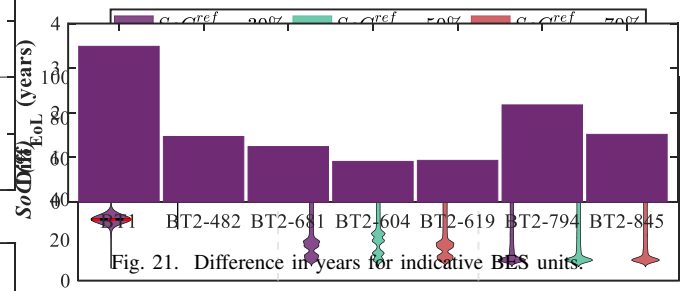

Fig. 21. Difference in years for indicative BES units.

V. Conclusion

The present work introduces a framework that provides the means for assessing the provision of ASs in LV DNs by PV-BES systems. PV-BES units providing either VR and PS services or only PS services are considered. The long-term impact of the BES capacity degradation on the effective provision of ASs is investigated on annual basis by conducting multiple 24-h quasi-static simulations. Therefore, due consideration is given on the appropriate modelling of the BES aging algorithm that is incorporated into the simulation model. These considerations are deemed important to replicate realistic operating conditions of the LV DN. To this extend, parametric investigations are conducted and their effects are quantified. The operating temperature, the SoC recovery signal, the adopted discharging strategy, the BES size and the simulation time resolution are considered as parameters in the analysis.

An application of the proposed framework to a modified version of the IEEE LV test feeder along with the results of the parametric analysis have shown that:

- The provision of both PS and VR services does not necessarily lead to accelerated BES capacity degradation compared to the case where only PS is considered.
- The adopted BES aging model is mainly influenced by the $\overline{SoC}$ operating value. Respectively, $\overline{SoC}$ is affected by the BES sizing characteristics and the employed discharging algorithm. In particular, decreased BES size results into increased $\overline{SoC}$, a wide SoC operating range and in turn to accelerated BES capacity degradation. In the same sense, both BES lifetime expectancy and grid performance are enhanced when the employed discharging strategy leads to low $\overline{SoC}$ values.
- To ensure efficient VR services for the whole lifetime of the PV units (20 years), at least one BES replacement must be considered.
- Higher operating BES temperature leads to a non-linear decrease of BES lifetime expectancy. However, due to

the accelerated BES aging, less BES units are available to provide VR hindering the reliable grid operation.

- The lifetime of BES units providing only PS services is mainly affected by the desirable SoC reference level of the recovery algorithm. Specifically, higher SoC_{bat}^{ref} values lead to increased $\overline{SoC}$ and consequently to decreased BES lifetime expectancy.
- Contrary to NFECs, the operating SoC can be used as a reliable index to evaluate the effect of different discharging strategies on the BES aging.
- During the planning phase, distribution system operators should determine the optimum BES sizing characteristics on the basis of both the BES cost and the network performance influenced by the BES lifetime.
- The time resolution of the BES aging analysis should be carefully selected to achieve a good estimation of the BES lifetime.

The proposed framework constitutes a holistic tool for DN utilities, aggregators as it allows the evaluation of the impact of BES degradation on the performance of ASs provided by PV-BES systems in any type of DN; thus enhancing the power system analysis and control of modern power systems.

REFERENCES

[1] K. D. Pippi, G. C. Kryonidis, A. I. Nousdilis, and T. A. Papadopoulos, "Assessing the provision of ancillary services considering bes capacity degradation," *2022 Int. Conf. Smart Energy Syst. Technol. (SEST)*, pp. 1–6, 2022.

[2] D. E. Olivares, A. Mehrizi-Sani, A. H. Etemadi, *et al.*, "Trends in Microgrid Control," *IEEE Trans. Smart Grid*, vol. 5, no. 4, pp. 1905–1919, 2014.

[3] A. Saint-Pierre and P. Mancarella, "Active Distribution System Management: A Dual-Horizon Scheduling Framework for DSO/TSO Interface Under Uncertainty," *IEEE Trans. Smart Grid*, vol. 8, no. 5, pp. 2186–2197, 2017.

[4] G. C. Kryonidis, E. O. Kontis, T. A. Papadopoulos, *et al.*, "Ancillary services in active distribution networks: A review of technological trends from operational and online analysis perspective," *Renew. Sustain. Energy Rev.*, vol. 147, p. 111198, 2021.

[5] Y. Wang, K. T. Tan, X. Y. Peng, and P. L. So, "Coordinated control of distributed energy-storage systems for voltage regulation in distribution networks," *IEEE Trans. Power Del.*, vol. 31, no. 3, pp. 1132–1141, 2016.

[6] M. Zeraati, E. M. G. Hamedani, and J. M. Guerrero, "A consensus-based cooperative control of pev battery and pv active power curtailment for voltage regulation in distribution networks," *IEEE Trans. Smart Grid*, vol. 10, no. 1, pp. 670–680, 2019.

[7] S. M. N. R. Abadi, A. Attarha, P. Scott, and S. Thiébaux, "Affinely adjustable robust volt/var control for distribution systems with high pv penetration," *IEEE Trans. Power Syst.*, vol. 36, no. 4, pp. 3238–3247, 2021.

[8] M. N. Kabir, Y. Mishra, G. Ledwich, *et al.*, "Improving voltage profile of residential distribution systems using rooftop PVs and Battery Energy Storage systems," *Applied Energy*, vol. 134, pp. 290–300, 2014.

[9] K. D. Pippi, G. C. Kryonidis, A. I. Nousdilis, and T. A. Papadopoulos, "A unified control strategy for voltage regulation and congestion management in active distribution networks," *Electr. Power Syst. Res.*, vol. 212, p. 108648, 2022.

[10] A. S. Zamzam, N. D. Sidiropoulos, and E. Dall'Anese, "Beyond relaxation and newton–raphson: Solving ac opf for multi-phase systems with renewables," *IEEE Trans. Smart Grid*, vol. 9, no. 5, pp. 3966–3975, 2018.

[11] H. Xu, A. D. Domínguez-García, V. V. Veeravalli, and P. W. Sauer, "Data-Driven Voltage Regulation in Radial Power Distribution Systems," *IEEE Trans. Power Syst.*, vol. 35, no. 3, pp. 2133–2143, 2020.

[12] E. Dall'Anese and A. Simonetto, "Optimal power flow pursuit," *IEEE Trans. Smart Grid*, vol. 9, no. 2, pp. 942–952, 2018.

[13] Y. Huang, "Day-Ahead Optimal Control of PEV Battery Storage Devices Taking Into Account the Voltage Regulation of the Residential Power Grid," *IEEE Trans. Power Syst.*, vol. 34, no. 6, pp. 4154–4167, 2019.

[14] R. Leng, Z. Li, and Y. Xu, "Two-stage stochastic programming for coordinated operation of distributed energy resources in unbalanced active distribution networks with diverse correlated uncertainties," *J. Modern Power Syst. Clean Energy*, vol. 11, no. 1, pp. 120–131, 2023.

[15] X. Li, D. Hui, and X. Lai, "Battery Energy Storage Station (BESS)-Based Smoothing Control of Photovoltaic (PV) and Wind Power Generation Fluctuations," *IEEE Trans. Sustain. Energy*, vol. 4, no. 2, pp. 464–473, 2013.

[16] L. Meng, T. Dragicevic, and J. M. Guerrero, "Adaptive Control Design for Autonomous Operation of Multiple Energy Storage Systems in Power Smoothing Applications," *IEEE Trans. Ind. Electron.*, vol. 65, no. 8, pp. 6612–6624, 2018.

[17] M. K. A. Atif, "Saviztky–Golay filtering for solar power smoothing and ramp rate reduction based on controlled battery energy storage," *IEEE Access*, vol. 8, pp. 33 806–33 817, 2020.

[18] M. K. M. A. Syed, "Moving regression filtering with battery state of charge feedback control for solar pv firming and ramp rate curtailment," *IEEE Access*, vol. 9, pp. 13 198–13 211, 2021.

[19] N. L. Y. Zhou, Z. Yan, "A novel state of charge feedback strategy in wind power smoothing based on short-term forecast and scenario analysis," *IEEE Trans. Sustain. Energy*, vol. 8, no. 2, pp. 870–879, 2017.

[20] G. C. Kryonidis, A. I. Nousdilis, K. D. Pippi, and T. A. Papadopoulos, "Impact of Power Smoothing Techniques on the Long-Term Performance of Battery Energy Storage Systems," in *2021 56th Int. Univ. Power Eng. Conf. (UPEC)*, 2021, pp. 1–6.

[21] A. I. Nousdilis, G. C. Kryonidis, T. A. Papadopoulos, "Comparative evaluation of solar power smoothing techniques considering battery degradation," *IEEE J. Photovolt.*, 2023, early access, doi: 10.1109/JPHOTOV.2023.3308259.

[22] L. Maeyaert, L. Vandevelde, and T. Doring, "Battery Storage for Ancillary Services in Smart Distribution Grids," *J. Energy Storage*, vol. 30, p. 101524, 2020.

[23] B. Xu, A. Oudalov, A. Ulbig, *et al.*, "Modeling of Lithium-Ion Battery Degradation for Cell Life Assessment," *IEEE Trans. Smart Grid*, vol. 9, no. 2, pp. 1131–1140, 2018.

[24] T. T. Mai, A. N. M. M. Haque, P. P. Vergara, *et al.*, "Adaptive coordination of sequential droop control for PV inverters to mitigate voltage rise in PV-Rich LV distribution networks," *Electr. Power Syst. Res.*, vol. 192, p. 106931, 2021.

[25] L. Zhang, Z. Mu, and C. Sun, "Remaining Useful Life Prediction for Lithium-Ion Batteries Based on Exponential Model and Particle Filter," *IEEE Access*, vol. 6, pp. 17 729–17 740, 2018.

[26] "IEEE Standard for interconnection and interoperability of distributed energy resources with associated electric power systems interfaces," *IEEE Std 1547-2018 (Revision of IEEE Std 1547-2003)*, pp. 1–138, 2018.

[27] A. Nieslony, "Rainflow counting algorithm." [Online]. Available: https://de.mathworks.com/matlabcentral/fileexchange/3026-rainflow-counting-algorithm,RetrievedJune8,2022.

[28] "European Low Voltage Test Feeder," Apr. 01, 2021. [Online]. [Online]. Available: https://site.ieee.org/pes-testfeeders/resources/

[29] R. C. Dugan and D. Montenegro, *Reference guide: The Open Distribution System Simulator*, Technical Report 9.0.0., Electrical Power Research Institute, Washington, DC, 2020.

[30] H. Hoffmann, "Violin Plot." [Online]. Available: https://www.mathworks.com/matlabcentral/fileexchange/45134-violin-plot,MATLABCentralFileExchange.RetrievedJanuary3,2023

[31] J. J. Kelly and P. G. Leahy, "Sizing battery energy storage systems: Using multi-objective optimization to overcome the investment scale problem of annual worth," *IEEE Trans. Sustain. Energy*, vol. 11, no. 4, pp. 2305–2314, 2020.

[32] K. D. Pippi, T. A. Papadopoulos, G. C. Kryonidis, and E. D. Kyriakopoulos, "The net-metering practice in medium-voltage pv-bes prosumers: A techno-economic analysis of the greek case," *Sustain. Energy, Grids and Networks*, vol. 36, p. 101156, 2023.